

JPMTR 064 | 1419  
DOI 10.14622/JPMTR-1419  
UDC 667.6 : 676.2

Research paper  
Received: 2014-07-15  
Accepted: 2015-08-28

## Effect of coating pigment, binder type and binder amount on planar liquid wicking on coated substrates

*Eveliina Jutila<sup>1</sup>, Risto Koivunen<sup>1</sup>, Patrick A. C. Gane<sup>1,2</sup>*

<sup>1</sup>School of Chemical Technology,  
Department of Forest Products Technology, Aalto University,  
PL 16400, 00076 Aalto, Finland

E-mail: eveliina.jutila@aalto.fi  
risto.koivunen@aalto.fi  
patrick.gane@omya.com

<sup>2</sup>Omya International AG, Baslerstrasse 42,  
CH-4665 Oftringen, Switzerland

### Abstract

This study focuses on the development of highly wicking coated substrates for microfluidic devices with enhanced resolution compared to current filter paper-based devices. Four highly absorbing pigments, fumed silica (FS), modified calcium carbonate (MCC), natural diatomite (ND) and flux-calcined diatomite (FCD), as well as three binders, styrene-acrylate (SA) latex, polyvinyl alcohol (PVOH) and carboxymethyl cellulose (CMC), were used to form coating structures with different wicking properties. Studies include characterisation of the pigment particles and thin layer wicking (TLW) experiments, in which wicking height of liquid in coatings is measured as a function of time. The results show that the choice of coating pigment and binder as well as the binder amount has a significant effect on wicking characteristics of a coating. The introduction of diatomite pigments into blends with MCC improved the wicking capabilities of the coating, especially in the case of ND. Latex was found to inhibit wicking of liquid the least, followed by PVOH and CMC. Increased binder amounts reduce wicking due to reduced pore connectivity and binder-filled pores. It was found that the wicking resistance of pigment alone is too high for rapid analysis over long distances in thick coatings. Once optimised for binder type and amount, these coating structures could be utilised as high resolution microfluidic analysis elements, i.e. test cells, incorporated either into a wicking channel matrix or placed at junctions of microfluidic channels derived from controlled hydrophobic/oleophobic printing or designed shrinkage fracture geometries.

**Keywords:** microfluidic device, absorbent coating, microdiagnostics, hydrophilic channel, printed functionality

## 1. Introduction

Microfluidic analytical devices represent one of the most promising future applications in functional printing. Paper-based devices are not only inexpensive and portable, but they can be modified easily and can provide a fast and simple analysis through capillary absorption without external instrumentation. Furthermore, the microfluidic character of the devices enables small sample volumes and simultaneous multianalyte sensing (Abe, Suzuki and Citterio, 2008). Researchers contributing to the majority of the prior art utilise cellulose-based chromatographic and filter papers, in which the sample wicks along cellulose fibres (Khan et al., 2010; Martinez et al., 2010; Yetisen, Akram and Lowe, 2013). Despite the practical advantages, current paperfluidic devices have limitations such as accuracy and sensitivity (Liana et al., 2012). By adopting porous coated substrates it may be possible to fabricate narrower, better spatially resolved channels, and so enhance the resolution and enable smaller volumes of sample to be applied, as well

as provide better colour contrast during optical sensing. The term resolution in this context refers to the degree of control of the spreading of liquids and printing inks, such as containment channel walls and sites used as test cells containing analytes in reaction areas, on the substrate used in microfluidic devices. Speciality coated substrates provide better resolution than uncoated filter paper devices, due to increased control over spreading via detailed design of pore structure and surface free energy. Previous attempts to use coated paper in paperfluidics, however, have proven unsatisfactory due to heterogeneous colour distribution in the reaction area and low wicking capabilities of coated paper (Määttänen et al., 2011; Zhong, Wang and Huang, 2012).

### 1.1 Background

A plain paper substrate can be transformed into a diagnostic device by printing functional components, such as

hydrophilic channels that guide polar fluid flow through analysis regions, points or cells to perform chemical assays, and by depositing chemical reagents into those test stations, the resultant components of which may even flow further into detection zones (Martinez et al., 2007; Mukhopadhyay, 2010). The main advantages of employing paper as a base material include its low cost, availability, portability and ease of modification. In addition, paper-based microfluidics function without external pumps, instrumentation or power, and provide a fast and simple analysis (Martinez et al., 2007), even remotely, if combined with an imaging device (Martinez et al., 2008; Yetisen, Akram and Lowe, 2013).

Low cost diagnostics are especially needed in underprivileged and developing countries, where people suffer from high levels of infectious diseases such as HIV, malaria and tuberculosis (Lee et al., 2010; Lisowski and Zarzycki, 2013) as well as in remote or other resource-limited areas distanced from healthcare establishments or electricity (Maxwell, Mazzeo and Whitesides, 2013). The microfluidic character of the devices enables reducing sample volume down to microlitres and, therefore, these devices offer a superior solution compared to conventional diagnostic tools, which often require large reagent and sample quantities as well as specific laboratory conditions and accomplished professionals for the analysis (Whitesides, 2013).

The basic principle of paperfluidic devices embodies the following three phases (Mukhopadhyay, 2010). First, a drop of sample, for example a bodily fluid, such as blood, is either placed on the device (planar laminar flow) or the device is dipped into the sample (wicking vertical flow). Secondly, the paper wicks the fluid through walled channels, derived from hydrophobic containment. Finally, the sample is guided into discrete detection zones. Most researchers utilise enzymatic or colour detection (Lisowski and Zarzycki, 2013),

though adopting gold nanoparticles (Mukhopadhyay, 2010) or electrochemical analysis offers an alternative detection method (Maxwell, Mazzeo and Whitesides, 2013; Yetisen, Akram and Lowe, 2013). Several research groups, including George Whitesides' research group at Harvard University (Martinez et al., 2007; 2010), Wei Shen's research group at Monash University (Khan et al., 2010; M. Li et al., 2012), as well as the Sentinel Bioactive Paper Network in Canada (Sentinel, 2015), amongst others, are actively developing simple devices for paper-based point-of-care (POC) diagnosis, food monitoring and environmental screening. Figure 1 shows a prototype of a paper-based device developed at Harvard University.

Despite the promising future of paper-based diagnostics and their many advantages, limitations such as accuracy and sensitivity still show that further development is required (Liana et al., 2012). The hydrophobic walled channels guiding the fluid flow are relatively wide, often greater than 200  $\mu\text{m}$ , hindering the liquid flow length for limited volume application. In addition, sample retention and evaporation during liquid transport result in insufficient sample delivery (Glavan et al., 2013; Li, Ballerini and Shen, 2012), and the resolution of the cellulose-based chromatographic or filter paper utilised by most researchers depends on the size and rather unstable dimensional stability of cellulose fibres in contact with water. Furthermore, swelling of cellulose fibres may further inhibit capillary flow (Yetisen, Akram and Lowe, 2013). By adopting coated substrates it may be possible to fabricate narrower, better spatially resolved channels, and so enhance the resolution and enable smaller volumes of sample to be applied. Also, paper thickness and colour may play a significant role in the analysis of the results (Yetisen, Akram and Lowe, 2013).

Previous attempts to use coated paper as a base material in printed microfluidic diagnostics have, however,

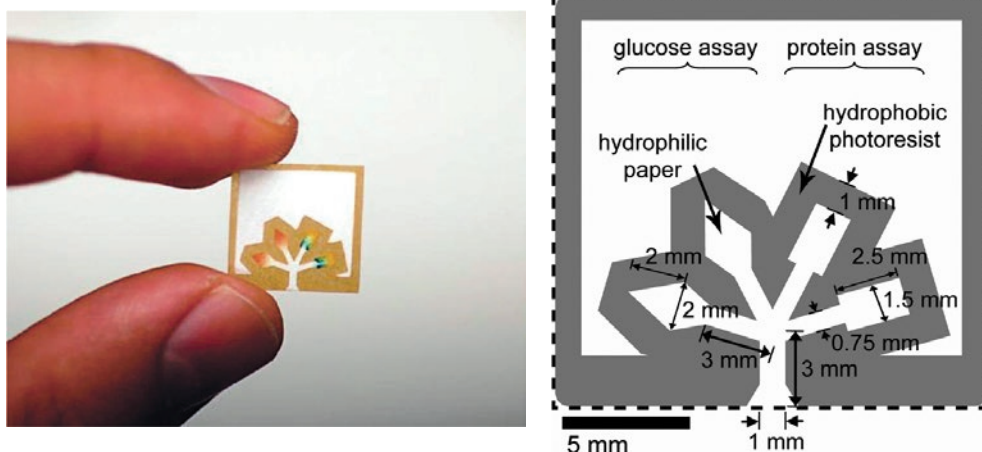


Figure 1: A prototype microfluidic device fabricated on filter paper for simultaneous analysis of glucose and proteins from urine (Reprinted with permission from Martinez et al., 2008; 2010. Copyright (2015) American Chemical Society)

proven unsatisfactory. Määttä et al. (2011) tested the performance of different hydrophilic paper substrates, including a highly permeable Whatman Grade 1 filter paper, an intermediate air permeance surface sized office copy paper, and a slow water and air permeance multilayer-coated paper substrate, for colorimetric glucose detection. The coated paper proved unsuitable for the colorimetric detection due to the heterogeneous colour distribution in the reaction area, caused by slow evaporation of the analyte solution. This phenomenon led to a considerable standard deviation in the calibration curve preventing accurate determination. However, coated paper was best suited for electrical applications, because it offers good print resolution compared to copy paper and filter paper. Zhong, Wang and Huang (2012) investigated the wicking potential of, and wax compatibility with, different paper substrates, including printing paper, paper napkins and paper towel. Their experiments showed that the printing paper had low wicking capability and suggested that this was due to its low porosity and adverse surface tension effects.

## 1.2 Principles of absorption

Paper-based diagnostics rely on wicking of liquid into the porous medium driven by capillary pressure, which is created by the difference in the surface energies of the dry and wetted solid matrices. Two approaches are commonly combined to model wicking mathematically: the classical Lucas–Washburn (L–W) equation combines the wetting force driving imbibition and the viscous drag opposing it. The viscous drag is related to the permeability defined by Darcy's law (Masoodi and Pillai, 2013). The L–W model assumes an hydraulic flow in an average single capillary derived from a bundle of aligned capillary tubes having the range of radii equivalent to the assumed pores in the sample (Lucas, 1918; Washburn, 1921), whereas Darcy's law describes permeation of an incompressible fluid through a saturated material under pressure as (i) a single-phase flow or (ii) two-phase flow through the porous substrates

## 2. Materials and methods

Coatings are constructed of various highly wettable pigments, bonded together and to the glass slide using a range of binder types.

### 2.1 Coating pigments, dispersants and binders

The chosen coating pigments consist of a highly porous form of *modified calcium carbonate* (MCC), typically used in the design of coated inkjet papers (Omyajet 5372 ME) provided by Omya International AG, Oftringen, Switzerland, *fumed silica* (FS, CAB-O-SPERSE PG002) provided by Cabot Corporation, Heverlee, Belgium, and two diatomaceous earths, *a natural diatomite* (ND,

where one phase replaces another (Masoodi and Pillai, 2013). Both of the phenomena constituting the L–W model assume equilibrium laminar flow. In complex micro and nano porous network structures, such as in coating structures, however, equilibrium is rarely established except after very long timescales and after relatively long wicking distances in respect to Darcy permeation behind the wetting front. This is because the liquid becomes accelerated and decelerated within the geometrically rapidly changing pore structure. To account for this, workers invoke either inertial effects via, for example, the Bosanquet equation (Bosanquet, 1923, Schoelkopf et al., 2000) or energy loss during pore entry flow (Szekely, Neumann and Chuang, 1971). The effect is to fill the finest pores in a given layer of the structure preferentially under linear time rate, and the larger pores slower under square root time rate, which in turn act as reservoirs for the next set of finest pores and so on (Ridgway and Gane, 2002). Once equilibrium is reached between these phenomena, a square root of time emerges as the macroscopic observation related to flow under permeation conditions (Ridgway and Gane, 2002). Yetisen, Akram and Lowe (2013) suggest that the most important parameters regarding wicking in porous materials include pore size, pore size distribution, porosity and surface area of the chosen substrate, as well as capillary flow rate, i.e. the migration speed of the liquid front moving along the test sample. Permeability is also needed to provide access to the differentiating mechanism of fine pores, and this contains the important factor of pore connectivity, which is strongly reduced by increasing binder content (Ridgway, Gane and Schoelkopf, 2006).

This study focuses on the development of highly wicking pigment coated substrates for microfluidic devices with enhanced resolution compared to current filter paper-based devices. Various highly absorbing coating pigments and different binders are used to form coating structures with different properties in regards to porosity, surface area and permeability.

Clarcel 78) and *a flux-calcined diatomite* (FCD, Clarcel FD), both supplied by Ceca Arkema, La Garenne-Colomber Cedex, France. MCC (52 % solids) and FS (20 % solids) were delivered as aqueous dispersions, whereas the diatomite pigments exist in powder form. The diatomite slurries were dispersed using *sodium polyacrylate salt* (Polysalz S, BASF, Ludwigshafen, Germany). *Carboxymethyl cellulose* (CMC, Finnfix 10, CP Kelco Oy, Äänekoski, Finland) was added to support dispersing and to provide both thickening and, at high dose, binding. CMC was prepared at 6 % solids by adding the required amount of CMC to cold water under agitation and heating the mixture in a slow cooker (Fiskars

Home, Hackman, Helsinki, Finland) to 50–60 °C. The solution was held at this temperature until the CMC had dissolved completely. The solution was allowed to cool down to room temperature before adding to the pre-slurried pigments under slow agitation.

The binders included a *styrene-acrylate latex* (SA latex, Acronal S 505, BASF, Ludwigshafen, Germany), having a particle size of approximately 0.2 µm and a  $T_g$  of < 1 °C, a *fully hydrolysed polyvinyl alcohol* (PVOH, BF-05 provided by Omya International AG), which has a degree of hydrolysis 98.5–99.2 mole %, and a molecular weight of 22 000–27 000 g·mol<sup>-1</sup> (Limpan et al., 2012), and CMC. PVOH was prepared at 10 % solids by adding the required amount of PVOH to cold water under agitation and heating the mixture in a slow cooker (Fiskars Home, Hackman, Helsinki, Finland) to 95–98 °C. The solution was held at this temperature until the PVOH had dissolved completely. The solution was allowed to cool down to room temperature before adding to the slurried pigments at a slow rate of agitation.

## 2.2 Substrates

Super premium microscope slides with ground edges (90°) made from low iron clear glass and having a thickness of 0.8–1.0 mm (25 × 75 mm, VWR International BVBA, Leuven, Belgium) were used as substrates in thin layer wicking (TLW) tests. The glass slides were attached to a 300 g·m<sup>-2</sup> liquid packaging board sheet (Stora Enso, Imatra, Finland) with double sided tape

(Scotch®, Suomen 3M Oy, Espoo, Finland) to ensure an even coating result. In addition, two commonly used filter papers, Whatman grades 1 and 4 (GE Healthcare Europe GmbH, Suomen sivuliike, Helsinki, Finland), were used as a comparison.

## 2.3 Coating colour formulations

The effect of different coating pigments on the wicking of liquid was tested using MCC and combinations of MCC with ND and FCD in a latex binder system. Table 1 presents the properties of the coating colours as well as the coating thickness and coat weight of coated samples. The coating thickness and coat weight were calculated by measuring thickness and the weight of the glass slides before and after coating. First, ND and FCD were blended with water to as high solids content as possible while retaining good “coatability”, after which MCC and binder was added to the diatomite-water mixture. In the case of ND this meant a solids content of 15.8 % (ND + MCC; 25 : 75) and 10.9 % (ND + MCC; 50 : 50), and in the case of FCD 37.7 % (FCD + MCC; 25 : 75) and 29.5 % (FCD + MCC; 50 : 50).

The effect of different binders and binder amounts on wicking of liquid was tested by using three different binders: SA latex and PVOH, which are commonly used binders, and CMC which is widely used as a co-binder in coating structures. Table 2 presents the properties of the coating colours as well as the thickness and coat weight of coated samples.

Table 1: Coating colour properties – different coating pigments with 4 pph latex; Brookfield spindle #4 was used with MCC, spindle #2 with other coating formulations

Coating formulation	Solids (%)	Thickness (µm)	Coat weight (g·m <sup>-2</sup> )	Brookfield visc. (mPa·s @ 100 min <sup>-1</sup> )	pH	Zeta poten. (mV)	Conductivity (µS·cm <sup>-1</sup> )
MCC (100)	52.00	50	60	402	8.49	-17.60	51.0
ND + MCC (25 : 75)	34.90	51	43	208	8.23	-18.60	39.7
ND + MCC (50 : 50)	19.20	46	43	66	8.03	-18.03	34.6
FCD + MCC (25 : 75)	48.60	72	63	130	8.49	-19.03	40.4
FCD + MCC (50 : 50)	39.50	71	49	42	8.83	-22.37	40.5

Table 2: Coating colour properties – different binders and binder amounts; Brookfield spindle #4 was used with all coating formulations

Coating formulation	Solids (%)	Thickness (µm)	Coat weight (g·m <sup>-2</sup> )	Brookfield visc. (mPa·s @ 100 min <sup>-1</sup> )	pH	Zeta poten. (mV)	Conductivity (µS·cm <sup>-1</sup> )
MCC	52.00	50	62	566	8.80	-16.57	43.4
MCC + 4 pph latex	51.92	74	62	402	8.49	-17.60	51.0
MCC + 8 pph latex	51.85	51	43	348	8.31	-17.80	41.3
MCC + 2 pph PVOH	48.00	42	52	884	8.50	-8.81	34.7
MCC + 10 pph PVOH	37.62	75	43	678	8.33	-7.47	40.2
MCC + 1 pph CMC	48.35	67	55	952	8.81	-18.30	38.4
MCC + 4 pph CMC	40.11	68	48	742	8.49	-22.70	45.9

## 2.4 Equipment

The particle size distributions of the coating pigments were determined by laser diffraction (Mastersizer 2000, Malvern Instruments Ltd., Malvern, UK), and the surface structures of the pigment particles were imaged with scanning electron microscopy (SEM). The surface area was supplied using an equivalent spherical particle model derived from the particle size distribution data as calculated from the Mastersizer.

For the SEM imaging, the coating samples were coated with a thin layer of gold using a table-top sputtering device (Leica EM SCD050, Leica Microsystems GmbH, Wetzlar, Germany) and analysed using a Hitachi TM-1000 SEM (Hitachi High-Technologies Europe GmbH, Krefeld, Germany).

The PVOH and CMC dispersions were prepared using a Heidolph RZR 1 mixer (Heidolph Instruments GmbH & Co, Schwabach, Germany). The coating colours were prepared in small sample containers and mixed by hand. The viscosity of the coating colours was measured using a Brookfield DV-II+ viscometer (Brookfield Engineering Laboratories, Inc., Massachusetts, USA) using spindles #2 and #4 and a rotation speed of  $100 \text{ min}^{-1}$ , the pH using a pH meter (Orion 420A, Thermo Scientific, Cambridgeshire, England), conductivity and zeta potential using a Zetasizer Nano-ZS90 (Malvern Instruments Ltd., Malvern, UK).

The glass slides were coated with the various test formulations using a K202 Control Coater (RK PrintCoat Instruments Ltd., Herts, UK) adopting the brown labelled wire-wound rod, which applies an  $80 \mu\text{m}$  thick wet film onto the substrate, with a speed setting of  $6 \text{ m} \cdot \text{min}^{-1}$ . The latex containing coated glass plates were dried in an oven at  $105 \text{ }^\circ\text{C}$  for 2 minutes to ensure proper latex film formation. The glass slides were weighed with a balance (Precisa XT 320M, Precisa Gravimetrics AG, Dietikon, Switzerland) and their

thickness measured with a caliper thickness tester (L&W Micrometer SE 250D, Lorenzen & Wettre, SE 164 93 Kista, Sweden) before and after coating to obtain coat weight and coating thickness.

A digital camera (Sony Cyber-shot DSC-HX20V, Sony Europe Limited, Espoo, Finland) was used to record images of the thin layer wicking tests as a function of time. The images were analysed using PowerPoint Picture and Drawing Tools (Microsoft Oy, Espoo, Finland). The coated glass slides were analysed with a light microscope (Leica DM750) coupled with a high definition digital camera (Leica ICC50 HD, Leica Microsystems GmbH, Wetzlar, Germany) and scanned with Epson Expression 1680 (Epson, Suwa, NGN, Japan).

## 2.5 Test set-up for thin layer wicking experiments

In thin layer wicking (experiments, a coated glass slide with 1 mm scaling marked on one side is lowered vertically into contact with the test liquid (10 % red food dye, Dr. Oetker Suomi Oy, Helsinki, Finland) and the wicking height (mm) is determined as a function of time (s).

Figure 2 shows a schematic of the wicking test set-up including the digital camera, a petri dish filled with dyed water to act as a liquid supersource, a transparent plastic support, e.g. a simple cup, holding the sample, the coated sample with 1 mm scale markings, and a light source (flashlight). Three repeats were made for each test. Wicking tests were conducted under standard paper testing conditions ( $23 \pm 1 \text{ }^\circ\text{C}$  and  $\text{RH } 50 \pm 2 \%$ ).

## 2.6 Test set-up for droplet wicking tests

Horizontal wicking was tested by placing a droplet of dyed water onto the coated samples with a pipette, as shown in Figure 3. The samples were scanned after reaching equilibrium and drying. The tests were conducted under standard paper testing conditions ( $23 \pm 1 \text{ }^\circ\text{C}$  and  $\text{RH } 50 \pm 2 \%$ ).

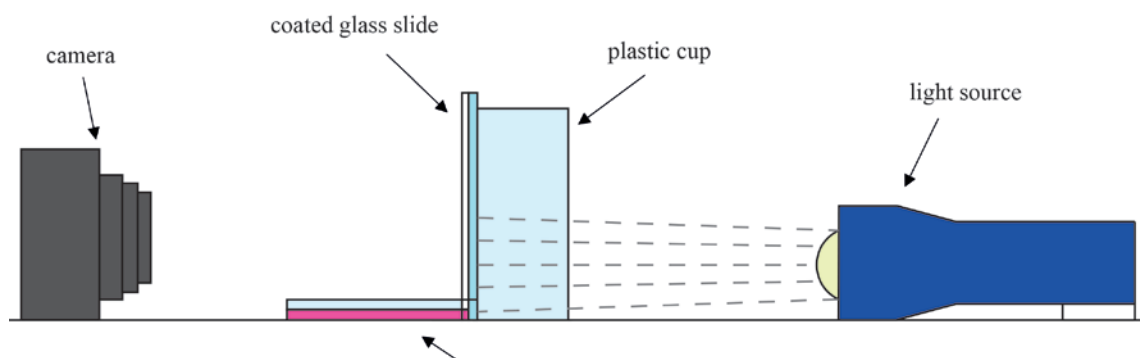


Figure 2: Schematic of the wicking test set-up

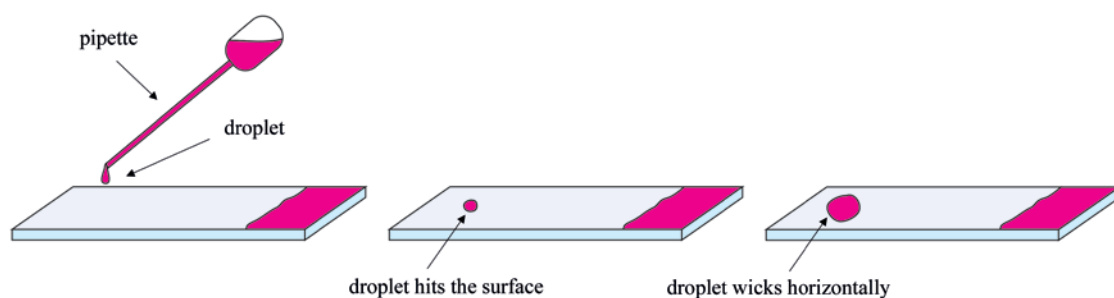


Figure 3: Schematic of the drop test set-up; additionally, the supersource wicking from the vertical test is also shown on the right side of each sample

### 3. Results

The findings from the experimental procedures are reported, beginning with the characterisation undertaken to define the likely properties of the pigments responsible for the surface interaction with liquid, followed by the direct observation of that interaction in respect to wicking in the porous structure of the resultant coatings, including the study of binder type and quantity used.

#### 3.1 Characterisation of the coating pigments

The volume frequency based particle size distributions of the coating pigments are shown in Figure 4, and the differences in particle size distributions are summarised in Table 3. Particle size distribution relates ultimately to the particle packing in the coating structure and affects the porosity and the permeability of the coating layer (Gane and Ridgway, 2007), thus influencing wicking of liquids in coatings containing the pigments. Fumed silica as coating pigment has a narrow particle size distribution and the individual pigment particles are the smallest of the four pigments studied. Silica, due to its micro-agglomerated nature, therefore, forms a less densely packed structure than either MCC, which has a spherical shape in a narrow size distribution, or diatomite pigments, having a broader particle size distribution, respectively, corresponding to a more tightly packed structure where small particles fill pores defined by the larger particles (Mueller, Osterhuber and Donigian, 2006). Studies have shown that smaller pores can be obtained using

fine broad particle size distribution pigment particles (Burri et al., 2004) and that the use of larger monosize particles results in both increased porosity and pore size in the final coating structure (Rousu et al., 2000).

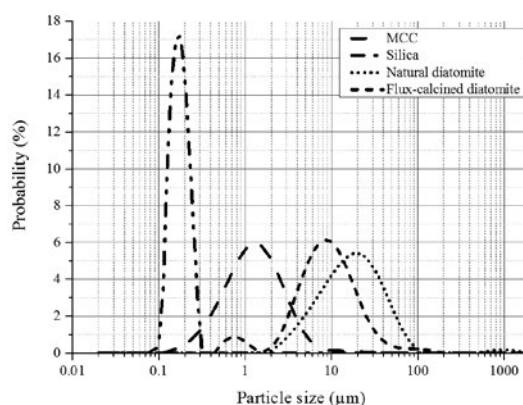


Figure 4: Volume frequency based particle size distribution of coating pigments

As we see in Table 3, the use of the equivalent spherical model for particle surface area, derived from the light scattering cross-section, greatly underestimates the true micro and mesoscale surface. To access the surface detail in this way would require the use of gas adsorption, e.g. nitrogen adsorption using the method BET of Brunauer, Emmett and Teller (1938). For example, the MCC is reported in the supplier's speci-

Table 3: Particle size and equivalent sphere model specific surface area of the coating pigments

Pigment	Specific surface area ( $\text{m}^2 \cdot \text{g}^{-1}$ )	Fine particle limit, $d_{10}$ ( $\mu\text{m}$ )	Median particle size, $d_{50}$ ( $\mu\text{m}$ )	Coarse particle limit, $d_{90}$ ( $\mu\text{m}$ )
MCC	6.20	0.47	1.33	3.445
FS	33.70	0.14	0.18	0.251
ND	0.36	5.88	18.25	49.604
FCD	0.88	3.32	9.16	24.429

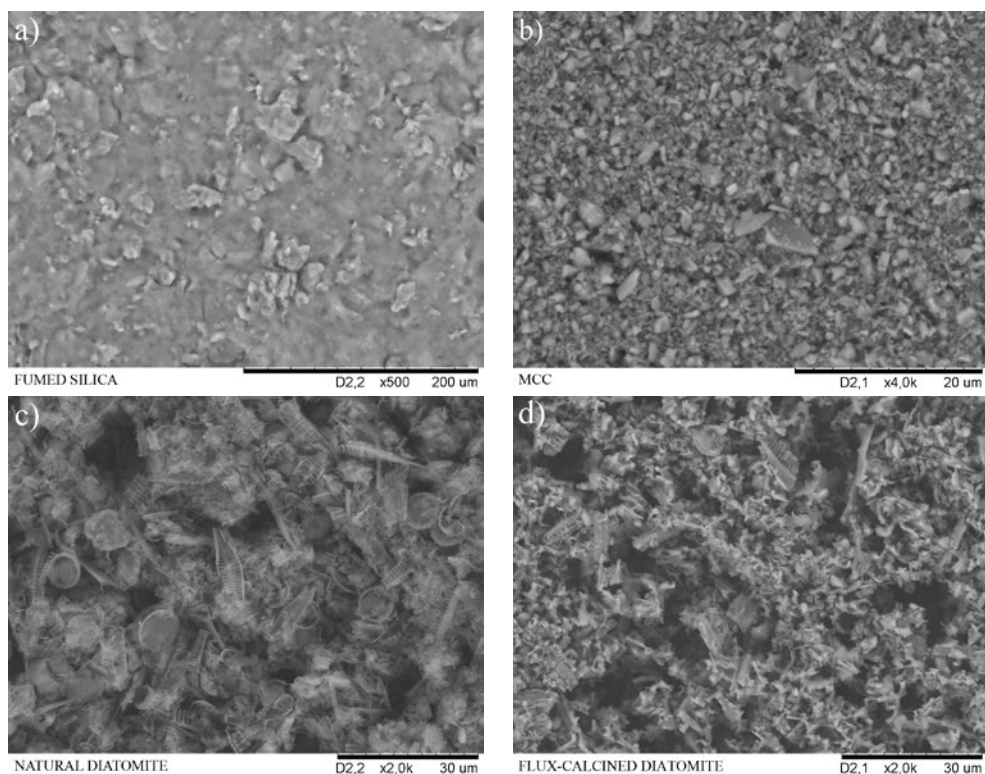


Figure 5: SEM images of the coating pigments: a) fumed silica, b) porous modified calcium carbonate (MCC), c) natural diatomite, and d) flux-calcined diatomite

cation to have a specific surface area ranging between  $\sim 30\text{--}40\text{ m}^2\cdot\text{g}^{-1}$  (Lamminmäki et al., 2009), and it is typical that fumed silica can have a specific surface area greater than or approximately  $100\text{ m}^2\cdot\text{g}^{-1}$ .

SEM images of the coating pigments are shown in Figure 5. Clear visual differences can be seen in the pigment particle size and shape. The diatomite pigment particles, especially the ND, are significantly larger than the finer MCC pigment and much finer silica particles, though the silica particles are seen to be partly clustered. The shape and size of the pigment particles also influence the void structure of the coating together with the chosen binder and binder amount.

### 3.2 Effect of pigment type on wicking

FS was selected as one of the coating pigments due to its known capacity to absorb large amounts of liquid in ratio to the solid volume as a result of its fine particle size and high level of microporosity generated in the clustered structure (Wu et al., 2012).

However, due to the ultrafine fraction and the resulting extremely high capillary forces during drying, shrinkage cracks formed in the coating and the coating layer peeled off upon drying, indicating adhesion failure when latex and PVOH were used as binders. Even the addition of MCC into the coating colour did not solve the problem

and therefore the silica pigment was discarded from the wicking experiments at this stage of the investigation.

The diatomite pigments were selected based on their potential absorption capabilities, although they are not conventionally used in paper coatings, being more commonly applied as filtration aids. However, experiments revealed that the chosen dispersing agent was not able to stabilise the coarse diatomite pigments against sedimentation. To overcome this, extensive amounts of CMC were required to retain the particles in suspension: 10 pph for ND and 12 pph for FCD. Although CMC solved the problem of pigment particle sedimentation, and improved the flow uniformity of the coating formulations, and hence coating coverage, it failed to prevent the formation of induced clumps during the coating process. This indicates that even CMC does not stabilise the pigment completely against shear-induced aggregation, and this can be considered as a characteristic of these pigments. The high amounts of CMC were seen, not unexpectedly, to interfere significantly with the wicking capabilities of the diatomite pigments. To achieve more stable coating colours while still utilising the diatomite pigments, ND and FCD were mixed with MCC.

Figure 6 shows the wicking height as a function of time when the various coating pigments or their combinations were tested with latex binder. Further, the impact of different binders and binder amounts, with MCC

pigment alone, was tested. The error bars represent the standard deviation of the observation. Three observations were made for each test. The wicking height was calculated from the difference between the final wicking height of the liquid and the initial wetting front.

The addition of diatomite pigments to MCC increased the wicking capabilities of the coatings significantly, especially in the case of the coarser ND. The MCC and ND + MCC coatings have similar thickness values, but ND containing coatings have significantly lower coat weight indicating a lower coating density. Furthermore, the solids content of the coatings containing diatomite are much lower than that of a coating consisting of MCC, but the formulations still produce thick coating layers. These factors indicate that the addition of larger diatomite particles creates a coating structure with larger voids compared to MCC. Although faster absorption of liquid is normally seen with finer pore structures over short distances (Gane, Matthews and Schoelkopf, 2000), in the case of diatomite a coating structure consisting of larger pigment particles led to greater wicking over the distances required for microfluidics, especially in these relatively thick coating layers. Diatomite structures internally have a low permeability, but they possess a very high porosity and the particles pack loosely together to provide well-connected flow pathways for wetting fluid resulting in low resistance to the flow generated by the capillary wall wetting forces (Akin et al., 2000). It is reported that the fine intraparticle pores and high surface area of the MCC act to provide strong wetting forces, which drive the meniscus forward (Ridgway and Gane, 2002), while the diatomite with its open interparticle packing reduces the resistance to viscous flow through the coating structure.

As we see in Figure 6, expressing the absorption/wicking height as a function of the square root of time does not deliver perfect straight lines, as would be the case if the traditional Lucas–Washburn model alone had

applied. We see first of all a short delayed rate of wicking, which reflects the likely depression of the contact meniscus as the sample is lowered into the supersource of liquid, which depends on the dynamic advancing contact angle, which becomes bigger as the sample is moved against the direction of wicking. Once equilibrium is reached, then a short period of linear root time behaviour is seen, followed by a slowing toward an eventual plateau. The plateau is defined as the equilibrium between wicking and evaporation at the far-reaches of the wetting meniscus. As we see from the optical analysis in Figure 7, this series of behaviours results in various concentration regions of dyestuff as the structure surface acts via adsorption, and the pore volume permits a balance between diffusion, bulk liquid flow and evaporation over the surface of the sample.

Figure 7 shows the wicking front and droplet spreading on and in the MCC and MCC-diatomite combination coating structures. The pigment surface interacts with certain dissolved materials, such as vegetable or insect dye, and thus the coating acts as a surface sorptive chromatographic column through surface and pore wall adsorption. This was evident during the experiments as a water front could be clearly observed ahead of the colorant front. The chromatographic effect was most prominent in the case of ND + MCC; 50 : 50, which showcased a series of lighter and darker areas. The lighter areas show incomplete pore filling or depletion of dye, whereas the darker coloured areas show saturated pores or concentration of dye. The innermost dark ring during droplet spreading marks the point at which there is no more surface liquid and the spreading proceeds subsurface due to the coating pore structure. The band of diffuse colour thereafter marks the adsorption of the dye onto the pore walls. The outermost intensely coloured ring is caused by evaporation of the liquid, which takes place faster than the onward wicking of the liquid, and so dye becomes concentrated – the so-called coffee stain effect. Similar layering effects can

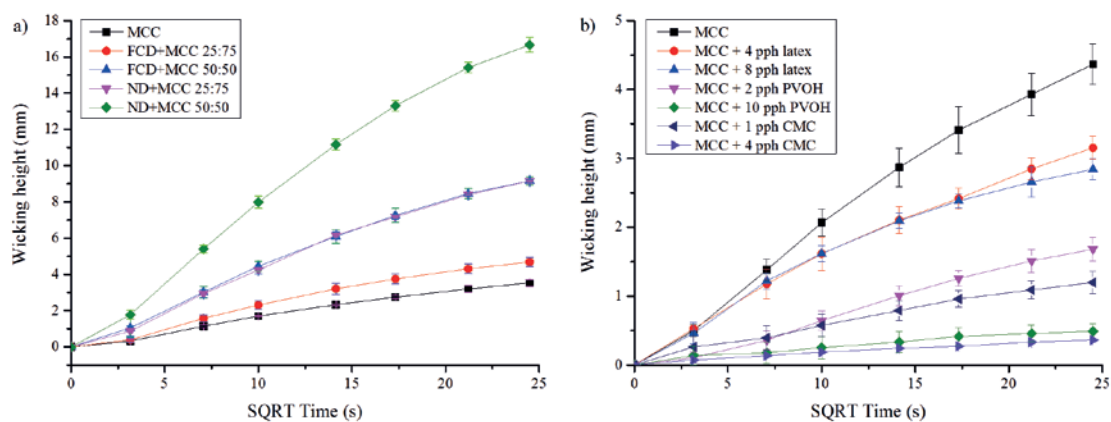


Figure 6: Wicking height as a function of square root of time ( $t^{0.5}$ ); a) when different coating pigment combinations were tested with 4 pph latex and b) when different binders and binder amounts were tested with MCC alone

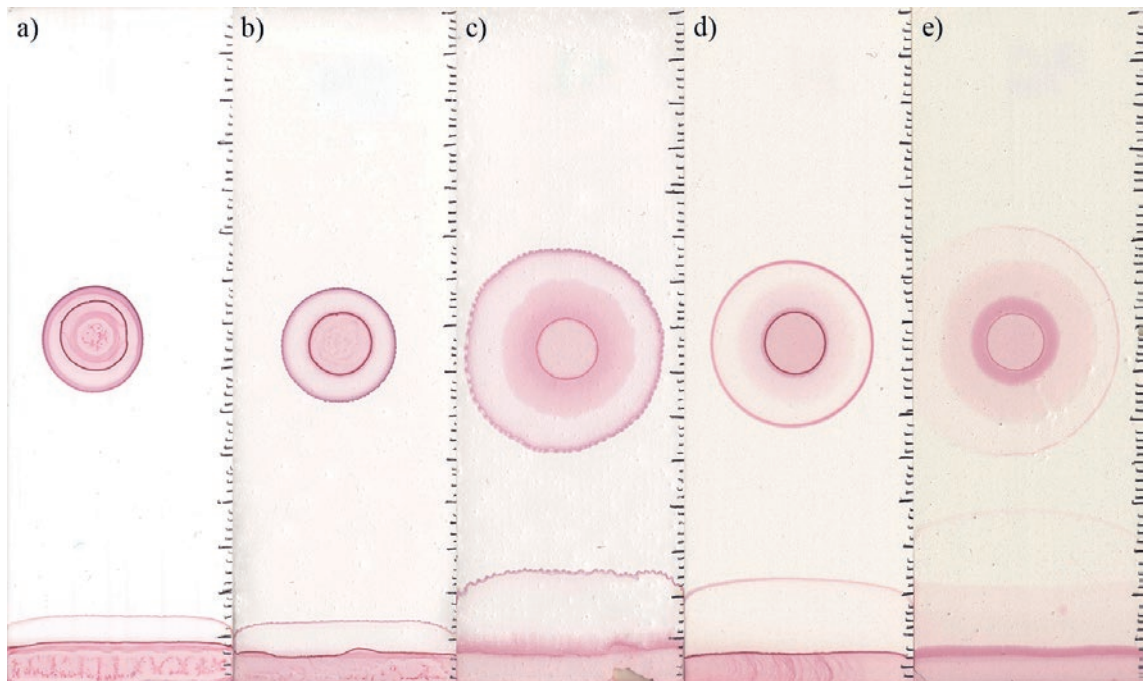


Figure 7: Wicking front and droplet spreading in a) MCC, b) FCD + MCC (25 : 75), c) FCD + MCC (50 : 50), d) ND + MCC (25 : 75) and e) ND + MCC (50 : 50) coating structures

be seen during the vertical wicking based on the identical series of events.

### 3.3 Effect of binder type and binder amount on wicking

The choice of a binder and the binder amount have a significant effect on wicking of liquid in a coating structure (as can be seen from Figure 6b), which presents the wicking height in the variously bound structures as a function of the square root of time. The highest wicking distance in the binder-containing coating systems was achieved with latex. An addition of 4 pph of latex provided sufficient binding to maintain the integrity of the coating and hindered the wicking remarkably less than PVOH and CMC. Further addition of latex (8 pph) reduced the wicking distance, but not too greatly. Latex may either change the pore structure by filling the pores and blocking the entrances affecting the capillary absorption (Burri et al., 2004) or at these lower doses actually undergoes depletion flocculation in the presence of pigment (Husband and Adams, 1993; Ridgway and Gane, 2007). Thus, a low level of suitable latex binder may lead to preservation of the total pore volume and permeability of the coating structure to a large extent (Ridgway, Kukkamö and Gane, 2011).

Even a low addition of PVOH (2 pph) reduced the wicking height noticeably, and the liquid front progressed even slower when a higher amount of PVOH (10 pph) was used, as expected. Significantly higher amounts of

PVOH would have been required to bind the coating properly onto the glass slides, but were not investigated since they would have inhibited wicking even more. The reason for low wicking distances in PVOH containing coatings most probably lies in PVOH's tendency to absorb water and swell, thus reducing the pore volume, especially affecting the fine high capillary pores and so reducing the pore network connectivity (Lamminmäki et al., 2011; Ridgway, Kukkamö and Gane, 2011). CMC also prevented liquid wicking significantly, but in addition failed to provide the required binding power to secure the coating onto the glass slide, even at higher dosage. This is probably due to the long timescale solubility of CMC in water.

Figure 8 shows the droplet spreading in the MCC coatings, when latex, PVOH and CMC were used as binders. The addition of a binder reduces the droplet spreading and dye migration by either filling some of the pores or, more particularly in the case of soluble binders, reducing the connectivity of the pore network as the soluble binders concentrate at the interstices of the pigment particle contact points due to capillary forces during the drying of the coating layer. Higher binder amounts result in less spreading and the dye concentrates in the edge areas. Once again, it can be seen that the dye does not spread homogeneously. The original equilibrium surface spread droplet size can be seen in the case of plain MCC (without binder) and in latex-containing coatings as an “inner ring”. As previously, the outer ring is related to the coffee stain effect

and associated Marangoni behaviour during evaporation. This delineation between surface equilibrium and internal pore wicking did not occur when soluble PVOH and CMC were used, although dye spreading was still not uniform, suggesting that the use of these soluble binders prevented a defined meniscus pinning line on the surface via a prevention of rapid evapora-

tion, such that the dye could continue to diffuse to the outer limit. This effect is thus related to the water swelling and dissolution properties of soluble binders. A more clearly visible outer coffee ring stain effect is seen as the soluble binder level is increased: the dye migrates and concentrates to the “outer rings” as the water evaporates.

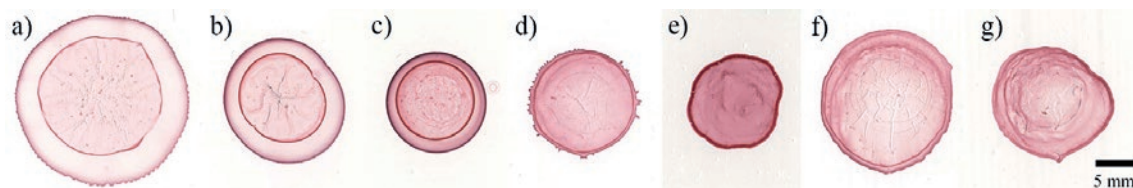


Figure 8: Droplet spreading in a) MCC, b) MCC + 4 ppb latex, c) MCC + 8 ppb latex, d) MCC + 2 ppb PVOH, e) MCC + 10 ppb PVOH, f) MCC + 1 ppb CMC and g) MCC + 4 ppb CMC

#### 4. Discussion

A number of interesting observations provide a deeper understanding of the relationship between the coating structure formation and the subsequent wicking tendency. Of perhaps greatest importance is the recognition of the role of wicking rate, and surface and binder chemistry, in respect to the distribution of soluble or carried substances in the liquid vehicle being wicked through the structure. On the one hand, surface adsorption by chromatography would prevent delivery to a diagnostic station, whilst, on the other hand, it could allow for valuable material separation to be undertaken. Similarly, the diffusion potential of dissolved constituents in the vehicle through soluble polymer binders, such as PVOH and CMC, could allow for

a more uniform deposition of a given solute, captured within the polymer matrix and then potentially eluted at a later date.

It is revealing to visualise the differences in macro and microstructure of the various resulting substrate materials. Figure 9 illustrates a comparison using optical microscopy between the large scale porous structure of a filter paper and the contrasting variation in microstructure seen between the fine MCC and the blends of MCC and the two diatomites. The lower permeability of the finer structures limits the long range wicking when considering using the complete coating layer as the absorbing structure.

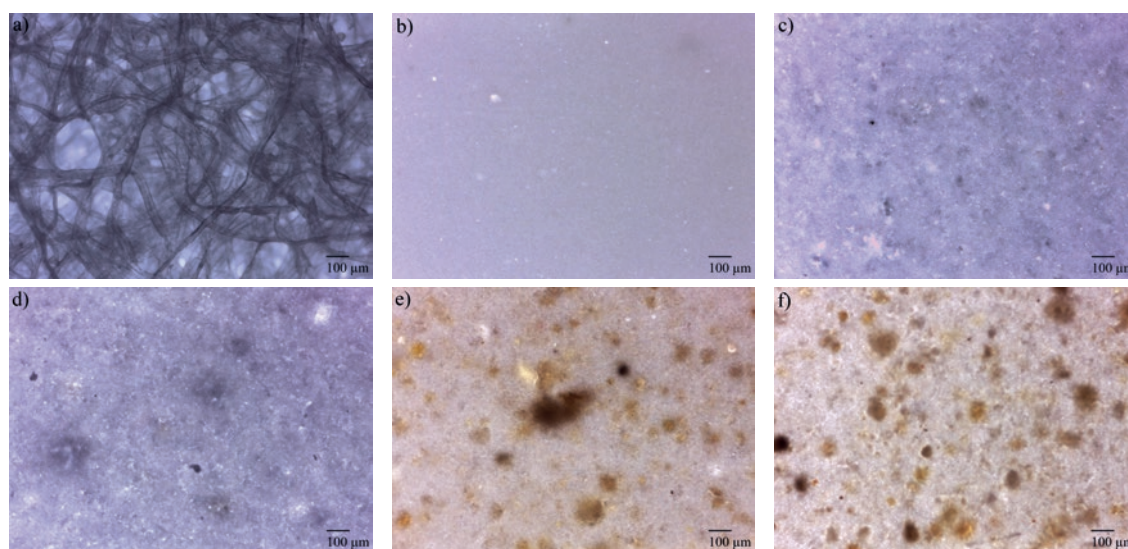


Figure 9: Light microscopy images of a) Whatman Grade 1 filter paper, b) MCC with 4 ppb latex, c) FCD + MCC (25 : 75), d) FCD + MCC (50 : 50), e) ND + MCC (25 : 75), and f) ND + MCC (50 : 50)

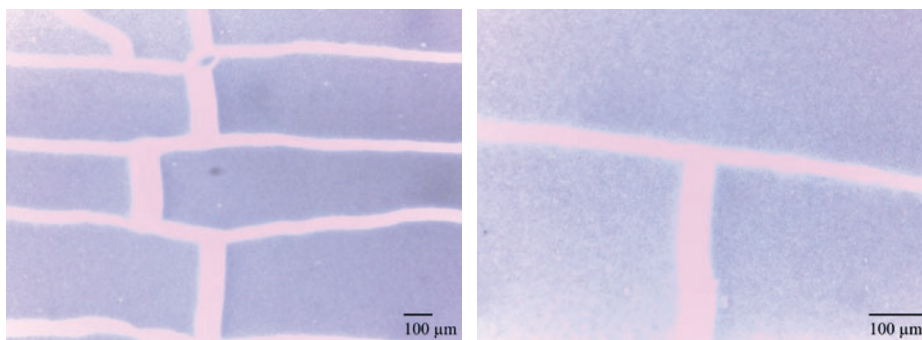


Figure 10: Light microscopy images of glass slides coated with fumed silica FS + MCC (25 : 50)

In the following discussion we concentrate on the direct physical relations between the wicking behaviour and the constituent formulations employed.

#### 4.1 Fumed silica

Neither latex nor PVOH were suitable for binding the silica onto the glass slides, and therefore the wicking capabilities of FS could not be studied at this point. Surface treatment of the glass slides or the use of other binders, especially inorganic binders, such as sodium silicate, could perhaps provide a worthwhile alternative, which could be studied. The cracking phenomenon of silica coatings could also perhaps be exploited by designing a certain substrate patterning that could lead to a coating structure that might provide geometrical “mud cracks” formed during shrinkage (Figure 10). The phenomenon could potentially be controlled by using different pigment and binder combinations, but would require further investigation.

#### 4.2 Dispersing diatomite pigments

Other stabilising agents against sedimentation and shear-induced aggregation could be researched to find an optimum to achieve a stable coating formulation whilst retaining the high wicking capabilities of the diatomite pigments. For example, the influence of using microfibrillated (MFC) or nanofibrillated (NFC) cellulose instead of CMC could be explored (Dimic-Misic et al., 2014). Alternatively, size selective sedimentation could be used to remove the coarsest (oversize) particles in a water-pigment mixture prior to coating to reduce the development of coating lumps.

#### 4.3 Effect of pigment type, binder type and amount on wicking

The coating structure, especially the packing, porosity, permeability and pore connectivity of the coating, can be altered significantly by using different pigments in combinations with different binders. In these experiments, the ND pigment containing coatings resulted in most wicking of the fluid, followed by FCD and MCC,

the latter itself being known to promote rapid absorption and high liquid uptake capacity (Ridgway, Gane and Schoelkopf, 2006). However, the challenge of fully utilising diatomite pigments lies in making the dispersions stable, as discussed earlier.

Liquid wicks up the coating structure faster when no binder is present, because binders fill or block some of the pores and/or pore connections in the coating structure, but nonetheless sufficient amounts of binder are required to bind the coating layer to the glass slide. The results agree with previous studies, in which higher binder levels of latex and PVOH reduce the absorption capabilities of the coating (Lamminmäki et al., 2009; Ridgway, Kukkamö and Gane, 2011).

The droplet spreading experiments of coated samples show that the spreading dye droplets does not result in a homogeneous distribution of the solute dye. The dye separates from the water chromatographically in the presence of different pigments (Figure 7) and binders (Figure 8). However, in the case of uncoated filter paper a more uniform solute distribution is seen (Figure 11), although some of the dye concentrates at the “outer ring”. This confirms the importance of understanding the interactive properties of the solute and the surface chemistry of the pore walls, as well as the distribution of liquid between the macroscopic coating surface and the microscopic pores. Similar observations about heterogeneous spreading on coated substrates have also been made by Määttänen et al. (2011).

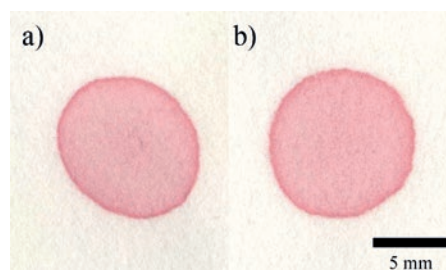


Figure 11: Droplet spreading on a) Whatman Grade 1 filter paper, b) Whatman Grade 4 filter paper

Furthermore, the thin layer wicking experiments showed that the wicking resistance of pigmented coatings, even without binder, is normally too high for rapid analysis over long distances in thick coatings. Zhong, Wang and Huang (2012) also concluded that coated paper did not possess good wicking properties. However, such coated papers are usually designed to prevent bleeding and spreading of ink. The selection of targeted coating formulation components, such as the coating pigments, binders and additives studied here, could be used to create a suitable coating for paperfluidic devices, especially when attention needs to be given to the potential for improved resolution at analysis/diagnostic stations when compared to uncoated fibrous substrates. Figure 12 shows an example of printed channel patterns on coated paper and on filter paper. It is evident that the ink spreads much less on the coated sample than on filter paper. This enables the printing of smaller channels and designs and, as a result, using smaller reagent volumes. Furthermore, advantageous use could be made of the surface chemistry and structure potential of coatings as media for solute or particulate suspension separation.

#### 4.4 Impact of the results on future applications

This study demonstrated how different pigments, binders and binder amounts affect wicking on coated sam-

ples. The desired wicking characteristics depend on the end purpose. In a microfluidic device, for example, the fluid needs to wick through the narrow channels all the way to the detection zones, and the spreading of the reagents printed/spotted onto the detection zones should be controlled so that the reagents do not migrate by further spreading to the channels. Also, homogeneous spreading of the reagent would be preferable. These both can be controlled by changing the point of assay design or using different coating formulations. Future publications will focus on studying wicking and drop spreading in such narrow coated channels and test designs.

Paper-based microfluidic devices offer a simple and an affordable option to existing laboratory-based tests. Furthermore, using coated paper as a substrate enables cost savings compared to filter paper due to decreased reagent and sample volumes and smaller device designs. The reagents and the sample will only have to penetrate through a thin coating layer, which can be followed by a barrier layer, instead of penetrating through the whole paper structure as in the case of filter paper. The resultant increased spatial resolution will greatly enhance the application in diagnostics and microfluidic devices, including microfluidic switches, for example.

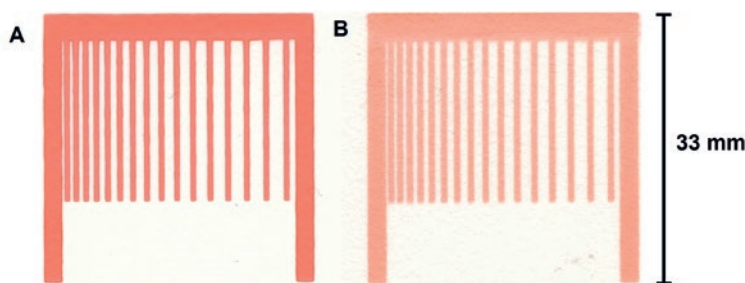


Figure 12. An example channel pattern printed on a) coated paper and b) filter paper (Koivunen et al., 2015)

## 5. Conclusions

The results show that the wicking characteristics of a coating can be greatly influenced by the choice of mineral coating pigment and binder – absorbent or non-absorbent. Using dyed water it could be shown that there is potential for using coatings to steer chromatographic or particulate separation of chosen solute components, as the coatings act as surface sorptive chromatographic columns through surface adsorption. Additionally, soluble binders can be used to provide potential differential

absorption for water and solute. Generally, however, the wicking resistance of pigment coatings is too high for rapid analysis over long distances. Once optimised for binder type and amount, these coating structures could be utilised as high resolution microfluidic analysis elements, i.e. test cells, incorporated either into a wicking channel matrix or placed at junctions of microfluidic channels derived from controlled hydrophobic/oleophobic printing or designed shrinkage fracture geometries.

## Acknowledgements

The fumed silica sample used in this study was provided free of charge by Cabot Corporation.

Funding for the project was provided by Omya International AG. Particle size distribution measurements were performed by Anu Anttila of Aalto University.

## References

- Abe, K., Suzuki, K. and Citterio, D., 2008. Inkjet-printed microfluidic multianalyte chemical sensing paper. *Analytical Chemistry*, 80(18), pp. 6928–6934.
- Akin, S., Schembre, J.M., Bhat, S.K. and Kovscek, A.R., 2000. Spontaneous imbibition characteristics of diatomite. *Journal of Petroleum Science and Engineering*, 25(3–4), pp. 149–165.
- Bosanquet, C.M., 1923. On the flow of liquids into capillary tubes. *Philosophical Magazine Series 6*, 45(267), pp. 525–531.
- Brunauer, S., Emmett, P.H. and Teller, E., 1938. Adsorption of gases in multimolecular layers. *Journal of American Chemical Society*, 1938, 60(2), pp. 309–319.
- Burri, P., Bluvoil, G., Gane, P.A.C. and Carlsson, R., 2004. Optimizing ink setting properties on double coated woodfree papers. In: *Proceedings of TAPPI Coating and Graphic Arts Conference*, May 16–19, 2004, Baltimore, USA: Tappi Press, pp. 201–216.
- Dimic-Misic, K., Ridgway, C., Maloney, T., Paltakari, J. and Gane, P., 2014. Influence on pore structure of micro/nanofibrillar cellulose in pigmented coating formulations. *Transport in Porous Media*, 103(2), pp. 155–179.
- Gane, P.A.C., Matthews, G.P. and Schoelkopf, J., 2000. Coating imbibition rate studies of offset inks: a novel determination of ink-on-paper viscosity and solids concentration using the ink tack force-time integral. In: *Proceedings of TAPPI International Printing & Graphic Arts Conference*, Atlanta, 3-10-2000, Savannah, US: Tappi Press, pp. 71–88.
- Gane, P.A.C. and Ridgway, C.J., 2008. Moisture pickup in calcium carbonate coatings structures: role of surface and pore structure geometry. In: *Proceedings of TAPPI 10<sup>th</sup> Advanced Coating Fundamentals Symposium*, June 10–13, 2008, Montreal, Canada, Atlanta, USA: Tappi Press, 13 p.
- Glavan, A.C., Martinez, R.V., Maxwell, E.J., Subramaniam, A.B., Nunes, R.M., Soh, S. and Whitesides, G.M., 2013. Rapid fabrication of pressure driven open-channel microfluidic devices in omniphobic R(F) paper. *Lab on a Chip*, 13(15), pp. 2922–2930.
- Husband, J.C. and Adams, J.M., 1993. Interactions in clay-based rotogravure coating colours. *Nordic Pulp and Paper Research Journal*, 8(1), pp. 195–199.
- Khan, M.S., Thouas, G., Shen, W., Whyte, G. and Garnier, G., 2010. Paper diagnostics for instantaneous blood typing. *Analytical Chemistry*, 82(10), pp. 4158–4164.
- Koivunen, R., Jutila, E., Bollström, R. and Gane, P., 2015. Inkjet printed reaction arrays on pigment coated substrates. In: *Proceedings of the 42<sup>nd</sup> International LARIGAI Conference*, Helsinki, Finland.
- Lamminmäki, T., Kettle, J.P., Puukko, P., Ridgway, C. and Gane, P.A.C., 2009. Inkjet print quality: the role of polyvinyl alcohol in speciality CaCO<sub>3</sub> coatings. *Journal of Pulp and Paper Science*, 35(3–4), pp. 137–147.
- Lee, W.G., Kim, Y-G., Chung, B.G., Demirci, U. and Khademhosseini, A., 2010. Nano/microfluidics for diagnosis of infectious diseases in developing countries. *Advanced Drug Delivery Reviews*, 62(4–5), pp. 449–457.
- Li, M., Tian, J., Al-Tamini, M. and Shen, W., 2012. Paper-based blood typing device that reports patient's blood type “in writing”. *Angewandte Chemie International Edition*, 51(22), pp. 5497–5501.
- Li, X., Ballerini, D.R. and Shen, W., 2012. A perspective on paper-based microfluidics: current status and future trends. *Biomicrofluidics*, 6(1), pp. 11301–1130113.
- Liana, D.D., Raguse, B., Gooding, J.J. and Chow, E., 2012. Recent advances in paper-based sensors. *Sensors*, 12(9), pp. 11505–11526.
- Limpan, N., Prodpran, T., Benjakul, S. and Prasarnpran, S., 2012. Influences of degree of hydrolysis and molecular weight of poly(vinyl alcohol) (PVA) on properties of fish myofibrillar protein/PVA blend films. *Food Hydrocolloids*, 29(1), pp. 226–233.
- Lisowski, P. and Zarzycki, P.K., 2013. Microfluidic paper-based analytical devices (μPADs) and micro total analysis systems (μTAS): development, applications and future trends. *Chromatographia*, 76, pp. 1201–1214.
- Lucas, R., 1918. Rate of capillary ascension of liquids. *Kolloid-Zeitschrift*, 23, pp. 15–22.
- Martinez, A.W., Phillips, S.T., Butte, M.J. and Whitesides, G.M., 2007. Patterned paper as a platform for inexpensive, low-volume, portable bioassays. *Angewandte Chemie International Edition*, 46(8), pp. 1318–1320.

- Martinez, A.W., Phillips, S.T., Carrilho, E., Thomas III, S.W., Sindi, H. and Whitesides, G.M., 2008. Simple telemedicine for developing regions: camera phones and paper-based microfluidic devices for real-time, off-site diagnosis. *Analytical Chemistry*, 80(10), pp. 3699–3707.
- Martinez, A.W., Phillips, S.T., Whitesides, G.M. and Carilho, E., 2010. Diagnostics for the developing world: microfluidic paper-based analytical devices. *Analytical Chemistry*, 82(1), pp. 3–10.
- Masoodi, R. and Pillai, K.M., eds., 2013. *Wicking in Porous Materials: Traditional and Modern Modeling Approaches*. Boca Raton: CRC Press/Taylor & Francis Group. 380 p.
- Maxwell, E.J., Mazzeo, A.D. and Whitesides, G.M., 2013. Paper-based electroanalytical devices for accessible diagnostic testing. *MRS Bulletin*, 38(04), pp. 309–314.
- Mueller, K., Osterhuber, E. and Donigian, D., 2006. When optimizing paper print performance, minerals matter. *Pulp & Paper*, 80(4), pp. 39–43.
- Mukhopadhyay, R., 2010. Paper-based diagnostics. *Chemistry World*, November 2010, pp. 50–53.
- Määttä, A., Fors, D., Wang, S., Valtakari, D., Ihalainen, P. and Peltonen, J., 2011. Paper-based planar reaction arrays for printed diagnostics. *Sensors and Actuators B: Chemical*, 160(1), pp. 1404–1412.
- Ridgway, C.J. and Gane, P.A.C., 2002. Dynamic absorption into simulated porous structures. *Colloids and Surfaces A: Physicochemical and Engineering Aspects*, 206(1–3), pp. 217–239.
- Ridgway, C.J. and Gane, P.A.C., 2007. Effect of latex and pigment volume concentrations on suspension and consolidated particle packing and coating strength. *Journal of Pulp and Paper Science*, 33(2), pp. 71–78.
- Ridgway, C.J., Gane, P.A.C. and Schoelkopf, J., 2006. Achieving rapid absorption and extensive liquid uptake capacity in porous structures by decoupling capillarity and permeability: nanoporous modified calcium carbonate. *Transport in Porous Media*, 63(2), pp. 239–259.
- Ridgway, C.J., Kukkamo, V. and Gane, P.A.C., 2011. Effects of binders and additives on inkjet coating pigment pore structures. In: *Proceedings of the TAPPI Coating and Graphic Arts Conference*, May 2011, Covington, USA: Tappi Press, pp. 1305–1319.
- Rousu, S.M., Gane, P.A.C., Spielmann, D.C. and Eklund, D., 2000. Separation of offset ink components during absorption into pigment coating structures. *Nordic Pulp and Paper Research Journal*, 15(5), pp. 527–535.
- Schoelkopf, J., Gane, P.A.C., Ridgway, C.J. and Matthews, G.P., 2000. Influence of inertia on liquid absorption into paper coating structures. *Nordic Pulp and Paper Research Journal*, 15(5), pp. 422–430.
- Sentinel Bioactive Paper Network. [online] Available at <www.bioactivepaper.com> [Accessed 12 September 2015].
- Szekely, J., Neumann, A.W. and Chuang, Y.K., 1971. The rate of capillary penetration and the applicability of the Washburn equation. *Journal of Colloid and Interface Science*, 35(2), pp. 273–278.
- Washburn, E.W., 1921. The dynamics of capillary flow. *Physical Review*, 17(3), pp. 273–283.
- Whitesides, G.M., 2013. Viewpoint on “Dissolvable fluidic time delays for programming multi-step assays in instrument-free paper diagnostics”. *Lab on a Chip*, 13(20), pp. 4004–4005.
- Wu, Y.-J., Lovell, V., Pekarovicova, A., Fleming, P.D. and Joyce, M., 2012. Influence of coating pigment porosity on inkjet color and lightfastness performance. *International Circular of Graphic Education and Research*, 5, pp. 6–17.
- Yetisen, A.K., Akram, M.S. and Lowe, C.R., 2013. Paper-based microfluidic point-of-care diagnostic devices. *Lab on a Chip*, 13(12), pp. 2210–2251.
- Zhong, Z.W., Wang, Z.P. and Huang, G.X.D., 2012. Investigation of wax and paper materials for the fabrication of paper-based microfluidic devices. *Microsystem Technologies*, 18(5), pp. 649–659.

## List of abbreviations

CMC	carboxymethyl cellulose	NFC	nanofibrillated cellulose
FCD	flux-calcined diatomite	POC	point-of-care
FS	fumed silica	PVOH	polyvinyl alcohol
MCC	modified calcium carbonate	SA	styrene-acrylate
MFC	microfibrillated cellulose	SEM	scanning electron microscopy
ND	natural diatomite	TLW	thin layer wicking